2012 American Control Conference
Fairmont Queen Elizabeth, Montréal, Canada
June 27-June 29, 2012

Nonlinear Parameter Estimation for Capacity Fade in Lithium-Ion Cells Based on a Reduced-Order Electrochemical Model

James Marcicki, Fabio Todeschini, Simona Onori and Marcello Canova

Abstract— **Lithium-ion batteries are central to the powertrain transformation taking place in the automotive industry, but the duration, cost, and complexity of experimental work for the characterization of aging mechanisms drive the need for models and model-based estimation approaches. This paper presents a model-based nonlinear parameter estimation method for the characterization of long-term capacity fade of Lithium-ion cells. The proposed approach relies on a reduced-order model of a LiC_6/$LiFePO_4$ cell, describing the mass and charge transfer in the solid and liquid phase, and the governing electrochemical principles. The model, validated with experimental data from a battery cell at beginning of life, is used to conduct a sensitivity analysis of the capacity to a subset of physicochemical parameters that are hypothesized to evolve throughout the battery's life. After isolating the most significant model parameters characterizing the long-term capacity degradation, experimental data from battery aging studies were used to solve a system identification problem to identify the degradation trend for the aging-related parameters. The developed tool is applicable to model-based diagnostic algorithms for ascertaining battery state-of-health and predicting the remaining useful life for Li-ion cells subjected to relevant usage and environmental conditions for automotive applications.**

I. INTRODUCTION

Lithium-ion (Li-ion) batteries are central to the powertrain transformation taking place in the transportation industry as a key technology for enabling the electrification of the automobile. However, a lingering concern with this chemistry is the overall durability, reliability and cycle life of the cells when subjected to diverse usage and environmental factors.

Battery cell manufacturers and system integrators must conduct extensive experimental activity in the design stage of an automotive battery pack to obtain an assessment of the aging process. Significant amounts of testing and validation are necessary prior to the introduction of any new technology for an automotive application, and Li-ion batteries are no exception. The length, cost, and complexity of such experiments drive the need for models and model-based estimation methods that are able to describe the aging process of the battery and predict the performance degradation.

In this scenario, predictive models based on electrochemical principles can be an effective support to understanding the underlying physicochemical mechanisms that cause capacity and power fade at the system level. While modeling, estimation and control for electrochemical energy storage systems have been the subject of extensive research over the past decades, there is still a lack of definitive, predictive understanding of the physicochemical processes that lead to the long-term degradation of the system, and in particular of the relationship between the life and usage conditions.

From an automotive perspective, operating conditions vary depending on the degree of hybridization of the vehicle [7]. With reference to plug-in hybrid electric (PHEV) or pure electric (EV) vehicles, it is critical to characterize the battery degradation phenomena resulting from sustained operation in the low State of Charge (SOC) region, and compare the aging that occurs under these conditions to studies conducted at other operating points [2], [1].

Some authors have applied non-linear regression to fit a subset of aging parameters to capacity test data at low rates [14]. Recently published work regarding the LiC_6/$LiFePO_4$ couple empirically analyzed the capacity fade rate for charge-depleting operation [6] and also examined the physicochemical mechanisms [19] using experimental characterization methods. A model-based analysis applied to characterize the aging process of the LiC_6/$LiFePO_4$ couple subjected to an automotive duty cycle may provide further opportunities for online state-of-health (SOH) estimation and prognostics in automotive applications.

With this goal in mind, this paper presents a model-based approach for nonlinear parameter estimation, with the objective of monitoring the long-term capacity fade of Lithium-ion cells. The proposed approach relies on a reduced-order model of a $LiFePO_4$/graphite cell, describing the mass and charge transfer in the solid and liquid phase, and governing electrochemical principles. The model is validated on experimental data from a battery cell at beginning of life (BOL). The model is applied to solve a system identification problem that identifies a degradation law for aging-related parameters. Parameter estimation is performed following a batch procedure using capacity test data from different stages of battery life. A relationship is established between the aging parameter set and the cell capacity, and validated using additional experimental data gathered during assessment tests of an aging campaign. The presented work is an initial step towards developing the capability to estimate capacity fade during automotive operating conditions.

II. DESCRIPTION OF THE ELECTROCHEMICAL MODEL

The proposed model structure follows from the single particle principle, which has been applied to both Li-ion and NiMH previously [4], [13], [15], [17]. The main modification

Fabio Todeschini is with Dipartimento di Elettronica ed Informazione, Politecnico di Milano, 20133 Milano, Italy. (todeschini@elet.polimi.it)

James Marcicki, Simona Onori and Marcello Canova are with the Center for Automotive Research, The Ohio State University, Columbus, OH, 43212, USA. (marcicki.1, onori.1, canova.1@osu.edu)

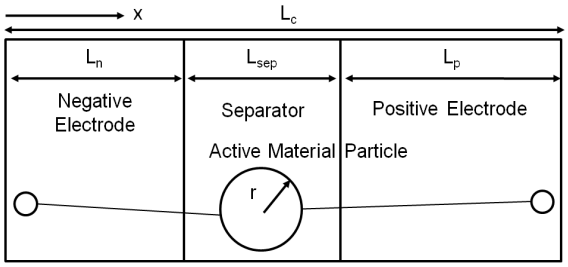

Fig. 1: Schematic of modeled unit cell showing linear diffusion in liquid phase and spherical diffusion in a representative particle.

to this structure is the inclusion of a time-varying resistance that accounts for the resistive reactant nature of the $LiFePO_4$ electrode [18]. This resistive reactant effect causes an increasing resistance with respect to depth-of-discharge during a current pulse response.

The model description begins with the output voltage ($V(t)$) definition,

$$\begin{aligned} V(t) =&(U_p(t) - U_n(t)) - V_r(t) - (\phi_e(L_c, t) - \phi_e(0, t)) \\ &- (\eta_p(t) - \eta_n(t)) - R_c I(t) - V_h(t) \end{aligned} \tag{1}$$

which states that the system is modeled by subtracting the overpotential that arises from various electrochemical phenomena from the time-varying open circuit voltage (OCV). The functional form of OCV for LiC_6 ($U_n(t)$) and $LiFePO_4$ ($U_p(t)$) is reported in [12], and good agreement is found for the system of this work.

As discussed in [11], a significant path dependence of the open circuit voltage for both $LiFePO_4$ and LiC_6 has been observed, leading to hysteresis. This phenomenon is modeled as a first order system with gain (H) and time constant (τ_h) that depend on SOC and temperature (T) [5]

$$\frac{dV_h}{dt} = \tau_h(T)|I|\left(H(SOC, sign(I), T) - V_h\right) \tag{2}$$

The three main forms of overpotential are ohmic, kinetic, and concentration, and these can occur in the solid or liquid phase. First, the overpotential associated with the solid phase is discussed. While ohmic overpotential may be neglected in the negative electrode due to the high conductivity of LiC_6 (>100 S/m), it is a significant loss in the positive electrode. The increasing resistance with depth of discharge of the $LiFePO_4$ electrode arises due to selectively charging or depleting the active material in an ohmically dominated fashion, such that the current density moves from areas with higher content of carbon coating to lower. This effect is accounted for with a resistance ($R_r(t)$) that increases with respect to depth of discharge, related to the conductivity of $LiFePO_4$ (σ_p) and the empirically defined conduction length ($L_{cond(t)}$) which increases in time with rate proportional to the current

$$R_r(t) = \sigma_p L_{cond}(t) \tag{3}$$

The ohmic loss from this resistance, along with a similar loss due to contact resistance (R_c) between the active material and current collector, are quantified as $V_r(t) = R_r(t)I(t)$ and $V_c(t) = R_c I(t)$ respectively.

Concentration overpotential in the solid phase occurs due to the limited ability of lithium ions to diffuse through the active material. It is modeled by solving the diffusion equation describing transport within a representative active material particle

$$\frac{\partial c_{s,i}}{\partial t} = \frac{D_{s,i}}{r^2}\frac{\partial}{\partial r}\left(r^2\frac{\partial c_{s,i}}{\partial r}\right) \tag{4}$$

The surface value of lithium concentration ($c_{s,i}(R_i, t)$) governs electrochemical behavior in lithium-ion batteries. Concentration overpotential results from the variation between the mean concentration and the surface value.

The kinetic overpotential is governed by the Butler-Volmer law. The intercalation current density ($j(x, t)$) is assumed constant with respect to space (x) in this work,

$$j_i(x, t) = j_i(t) = \frac{I(t)}{AL_i\epsilon_i} \tag{5}$$

where AL_i denotes the electrode volume and ϵ_i is the active material volume fraction of the electrode. Inverting the Butler-Volmer law leads to the expression for kinetic overpotential

$$\eta_i = \frac{\bar{R}T}{\alpha F} sinh^{-1}\left(\frac{j_i(t)}{2a_i k_i\sqrt{c_{s,i}(R_i)c_e(c_{max,i} - c_{s,i}(R_i))}}\right) \tag{6}$$

Increased values of the kinetic rate constants (k_i) will lead to decreased kinetic overpotential. As the surface concentration approaches the saturation value ($c_{max,i}$), the kinetic overpotential increases.

The liquid phase contains ohmic and concentration sources of overpotential. The governing equation of transport within the liquid is [9]

$$\frac{\partial c_e}{\partial t} = D_e\frac{\partial^2 c_e}{\partial x^2} + j(x, t) \tag{7}$$

where the intercalation current is piecewise constant, defined by Eq. (5) in the positive and negative electrode and taking a value of zero in the separator region. The potential is dependent upon the concentration according to

$$\frac{\partial \phi_e}{\partial x} = -\frac{i_e}{\kappa} + \frac{\bar{R}T(1 - t_0^+)}{F}(1 + \beta)\frac{\partial ln(c_e)}{\partial x} \tag{8}$$

The activity coefficient (β) is treated as a tunable constant parameter. The potential at $x = 0$ is set to zero, which implies only potential differences are considered relevant. Then Eq. (8) may be integrated directly to obtain the potential difference between $x = 0$ and $x = L_c$ after solving Eq. (7).

Finally, the cell capacity (Q) predicted by the model is defined as the sum of charge removed from the cell within specified voltage limits:

$$Q = \int_0^{t_f} I(t)\, dt \tag{9}$$

where the total time of discharge t_f is determined based on elapsed time when the lower cell voltage limit is reached.

TABLE I: Discharge capacity sensitivity summary.

Parameter	$S(Q)$
z_0	1.01×10^0
y_0	0
ϵ_n	1.01×10^0
ϵ_p	2.92×10^{-4}
$z_0 \cup \epsilon_n$	1.92×10^0
$z_0 \cup y_0$	1.01×10^0
$z_0 \cup \epsilon_p$	1.01×10^0
$\epsilon_n \cup y_0$	1.01×10^0
$\epsilon_n \cup \epsilon_p$	1.01×10^0
$\epsilon_p \cup y_0$	2.92×10^{-4}
$z_0 \cup \epsilon_n \cup y_0$	1.92×10^0
$z_0 \cup \epsilon_n \cup \epsilon_p$	1.92×10^0
$z_0 \cup \epsilon_p \cup y_0$	1.01×10^0
$\epsilon_n \cup \epsilon_p \cup y_0$	1.01×10^0
$z_0 \cup y_0 \cup \epsilon_n \cup \epsilon_p$	1.92×10^0

TABLE II: ANR26650 cell specifications.

Cathode Active Material	$LiFePO_4$
Anode Active Material	LiC_6
Nominal Capacity	2.3 Ah
Nominal Voltage	3.3 V
Internal Impedance	8 mΩ
Maximum Continuous Discharge	70 A
Maximum Pulse Discharge (10 seconds)	120 A

TABLE III: Specifications for aging characterization of the cells considered in this work.

Factor	Cell 1	Cell 2	Cell 3
Cell Surface Temperature	55^oC	55^oC	55^oC
SOC Range	0 - 30%	0 - 10%	0 - 20 %
Current Rate	2C	2C	2C

III. SENSITIVITY ANALYSIS

A sensitivity study was conducted to examine the main factors and factor interactions that could contribute to capacity fade, based on the described model. The parameter subset is chosen as the active material volume fractions in the positive and negative (ϵ_p and ϵ_n, respectively), and the initial amount of cyclable lithium in the positive (y_0) and negative (z_0) normalized by the saturation value. These four parameters have been deemed significant by prior work [8]. To compute the sensitivity, the model capacity prediction is determined using the nominal parameter set and a parameter set perturbed by 10% (ΔP). The sensitivity of capacity with respect to each parameter is

$$S(Q) = \frac{\Delta Q/Q}{\Delta P/P} \tag{10}$$

Table I summarizes the results of the sensitivity study when including factor interactions for discharge capacity.

Based on this preliminary analysis, it appears that the discharge capacity is not correlated to the positive electrode parameters. While these parameters have a noticeable effect on the charge capacity, they are effectively unobservable during discharge due to the two-phase nature of the $LiFePO_4$ electrode and the cell composition ranges. For this reason they can be removed from the parameter identification process, but devising methods for identifying the aging properties of the positive electrode will be the subject of future work.

IV. EXPERIMENTAL ANALYSIS AND MODEL VALIDATION

In order to evaluate system-level capacity and power fade, a battery aging campaign was conducted at the Center of Automotive Research (CAR), using $LiFePO_4$ cells produced by A123. Table II summarizes the main specifications for the cell considered in the study.

The cell terminal voltage, current, and temperature have been recorded using a sample frequency of 10 Hz. The aging campaign conducted on the cells consists of charge/discharge cycling while controlling the cell surface temperature at $55°C$ using a Peltier junction. This elevated temperature is chosen to accelerate the degradation process while ideally maintaining the same degradation mode as typical automotive operating conditions. Depth-of-discharge and current rate are varied using a full factorial design-of-experiments approach to investigate the effect of each factor on the performance degradation rate. State of charge information is obtained by post-processing the measured current throughput of the cell, and the duty cycle current is controlled to produce a triangular SOC waveform between selected maximum ($\overline{\text{SOC}}$) and minimum ($\underline{\text{SOC}}$) values. For this study, data from three Li-ion cells are used with aging protocols summarized in Table III. An example of the input current profile used for the aging cycles of Cell 1 and the calculated SOC are plotted in Fig. 2.

Using the voltage and current data from the aging experiments, the electrochemical cell model was validated. The initial parameter values were identified at the beginning of battery life using a combination of current pulse data and applying the estimation techniques described in this section to a BOL capacity test. The model prediction compared with experimental data is given in Fig. 3.

The relaxation dynamics after the lower voltage limit is reached are not captured accurately due to an unknown and difficult to characterize amount of hysteresis as SOC

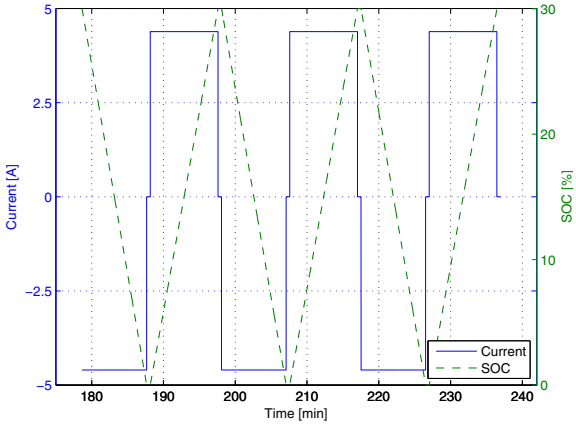

Fig. 2: Current and SOC profile during aging campaign of Cell 1.

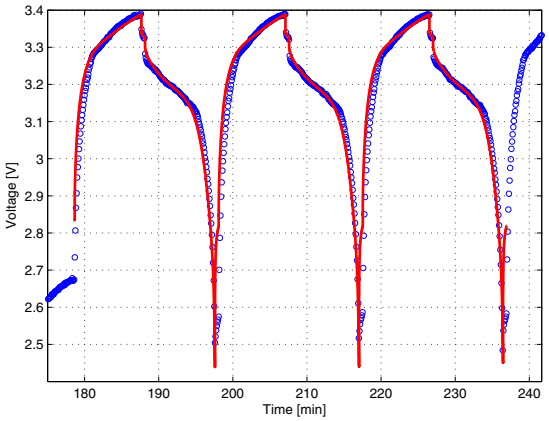

Fig. 3: Comparison of predicted voltage (line) and experimental data (points) during cycling. Current input is from Fig. 2.

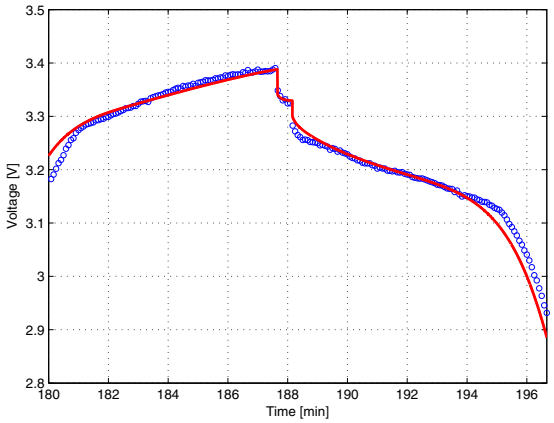

Fig. 4: Detailed comparison of predicted voltage (line) and experimental data (points) showing onset of voltage knee and relaxation following charge interval.

approaches zero. However, good agreement is obtained during the relaxation following the charge current pulse and throughout the discharge phase. Furthermore the onset of the voltage knee that effectively limits the discharge capacity is predicted well, and prediction of voltage during charge converges as SOC increases. Fig. 4 displays these aspects in greater detail.

During the aging campaign, capacity assessment tests were periodically recorded beginning with battery BOL and at specified current throughput intervals. The capacity assessment tests were conducted by first charging the cell using a constant current of 1C, followed by a 45 minute constant voltage hold at 3.6 V as specified by the manufacturer. Then, a complete discharge is performed on the cell at a constant current of 1C until the lower voltage limit of 2.5 V is reached. During each assessment, the cell surface temperature was maintained at 55^oC.

V. NONLINEAR ESTIMATION OF CELL AGING PARAMETERS

A nonlinear estimation procedure was defined based on the reduced-order electrochemical model to obtain the evolution

TABLE IV: Bounds for parameter estimation algorithm.

Parameter	Upper Bound	Lower Bound
z_0	0.5	0.9
ϵ_n	0.2	0.7
σ_p	0	0.5

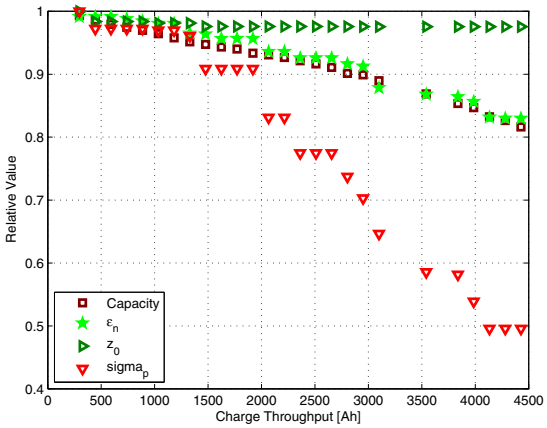

Fig. 5: Capacity degradation and results of parameter estimation process (data from Cell 1).

of the aging parameter set throughout the cell life. Based on the preliminary sensitivity analysis and results available in the literature [14], [19], [10], the normalized initial lithium concentration in the anode, z_0, and the active volume fraction ϵ_n were considered as the parameters that mostly affect the capacity degradation. In addition, the conductivity σ_p of the positive electrode is included in the parameter set to account for the noticeable increase in slope of the normally flat discharge curve for the batteries used in this work. The conductivity decrease during aging is expected and most likely has a role in power fade as well.

A nonlinear least square procedure is implemented based on the trust region reflective algorithm [3], [16]. The algorithm consists of finding the optimal set of parameters $\vec{P}^* = [z_0^*, \epsilon_n^*, \sigma_p^*]$ minimizing the cost function in Eq.(11), where the error $\vec{e}$ is a vector of differences between the experimental data and the predicted voltage ($\hat{e}(t) = V_{exp}(t) - V(t)$). The nonlinear least square problem is cast as:

$$\vec{P}^* = \underset{[z_0,\epsilon_n,\sigma_p]}{\operatorname{argmin}} \left(\frac{1}{2} (\Delta\vec{P})^T \frac{\partial^2 \vec{e}}{\partial \vec{P}^2} (\Delta\vec{P}) + (\Delta\vec{P})^T \frac{\partial \vec{e}}{\partial \vec{P}} \right) \quad (11)$$

The gradients of Eq. (11) are computed using a finite-difference approach. The adaptation of the aging parameter vector is based on Eq. (12)

$$\begin{aligned} &\text{If } \vec{e}(\vec{P} + \Delta\vec{P}) < \vec{e}(\vec{P}), \;\; \vec{P} = \vec{P} + \Delta\vec{P} \\ &\text{Else } \vec{P} = \vec{P} \end{aligned} \quad (12)$$

The trust region reflective algorithm is particularly advantageous because it allows for bounded estimation and the aging parameters in question have physical boundaries. The applied parameter bounds are summarized in Table IV.

The parameter identification results and measured capacity for the entire cycle life of the cell are in Fig. 5.

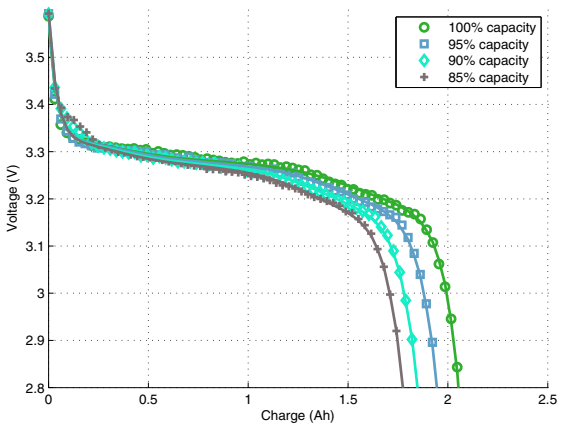

Fig. 6: Discharge curves obtained during BOL, EOL, and two intermediate capacity tests, comparing experimental measurements (points) and model estimates (lines). Data from Cell 1

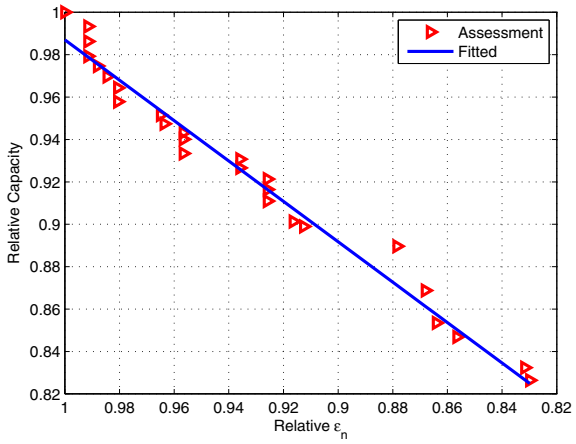

Fig. 7: Cell capacity measured experimentally during assessment test versus active material volume fraction of the negative electrode, as identified from the estimation procedure (data from Cell 1).

The normalized amount of cyclable lithium is roughly constant for the cell examined in Fig. 5. Both the active material volume fraction and conductivity have a decreasing trend with respect to charge throughput; however, the decrease in conductivity is noticeably larger. The decrease of active material is in agreement with experimental studies from literature [19] which state that active material loss in the negative electrode can be a significant source of performance degradation in the $LiC_6/LiFePO_4$ system. Note that even though the normalized amount of cyclable lithium is constant, the decreasing amount of active material implies that the actual amount of cyclable lithium is also decreasing. Further detailed analysis is needed to identify the mechanisms underlying these trends.

Fig. 6, compares the model voltage prediction to the capacity test data from BOL, two intermediate stages of testing, and end of life (EOL). As expected, the cell capacity progressively decreases as aging cycles continue towards EOL. For clarity, results from four capacity assessments are plotted, though data were recorded for several more intermediate stages between BOL and EOL.

As Fig. 6 shows, good agreement is obtained at all stages of cell life, with maximum error of approximately 20mV between model prediction and experimentally measured voltage. From a system standpoint, the apparent close correlation between the active material volume fraction and the cell capacity suggested by Fig. 5 is quite useful. Fig. 7 examines this correlation in greater detail, while also displaying a plotted linear fit

$$Q = 0.953\epsilon_n + 0.034 \tag{13}$$

Recall that the conductivity was included only to reduce the RMS error between experimental and model voltage prediction. Therefore, even though it does tend to decrease during aging, it is not included in the capacity regression.

To validate the correlation between the active material volume fraction and the cell capacity, the process is repeated for a two additional cells from the broader aging campaign, whose test specifications are summarized in Table III. First

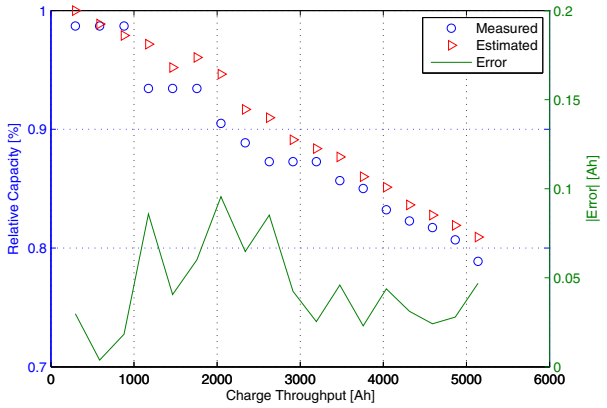

Fig. 8: Comparison of measured and estimated cell capacity from ϵ_n versus charge throughput (left-axis), and estimation error versus charge throughput (right axis). Data from Cell 2.

the active material volume fraction (and the other aging parameters) are estimated using the process applied previously. Then Eq. (13) is used to give an estimate of the capacity measured during each assessment test for the second cell. Finally the estimated capacity and experimentally measured capacity are compared in Fig. 8 to provide evidence for the utility of the correlation.

The predicted capacity is generally within 0.1 Ah of the actual value using this approach, which is useful considering cell-to-cell capacity variations are always present as well.

The utility of this finding lies in the fundamental significance of capacity versus that of the active material volume fraction. Capacity is a concept defining the amount of charge contained in an electrochemical energy storage device between specified voltage limits. The volume fraction is an actual physical parameter which effects the electrical dynamics of the cell, and as such it may be possible to estimate its value from voltage and current measurements. Combined with an open loop model for capacity fade, accurate online estimation of cell capacity may be possible.

VI. CONCLUSIONS AND FUTURE WORK

In this paper, a reduced-order model has been presented and used to solve a non-linear parameter estimation problem for characterization of capacity fade in lithium ion batteries. After conducting a sensitivity analysis of the discharge capacity with respect to several model parameters, a set of aging parameters were identified, namely describing the active material volume fraction, and the initial amount of cyclable lithium.

The result of the parameter estimation is that capacity is correlated to a physical parameter that is observable from the cell output voltage. This suggests it is possible to perform estimation of capacity from the battery current-voltage dynamics without performing a distinct capacity test, a result that is significant for the estimation of battery SOC and SOH for hybrid electric vehicle applications. Future work will focus on developing estimation algorithms for SOH and investigating prognostics methods.

VII. ACKNOWLEDGMENTS

The authors gratefully acknowledge the CAR Industrial Consortium and the Ford University Research Project program for their support.

REFERENCES

[1] D. Abraham, J. Knuth, D. Dees, I. Bloom, and J. Christophersen, "Performance degradation of high-power lithium-ion cells – Electrochemistry of harvested electrodes," *Journal of Power Sources*, vol. 170, no. 2, pp. 465 – 475, 2007.

[2] S. Bourlot, P. Blanchard, and S. Robert, "Investigation of aging mechanisms of high power li-ion cells used for hybrid electric vehicles," *Journal of Power Sources*, vol. 196, pp. 6841 – 6846, 2011.

[3] T. Coleman and Y. Li, "On the convergence of interior-reflective newton methods for nonlinear minimization subject to bounds," *Mathematical Programming*, vol. 67, no. 1, pp. 189 – 224, 1994.

[4] B. Haran, B. Popov, and R. White, "Theoretical analysis of metal hydride electrodes," *Journal of The Electrochemical Society*, vol. 145, no. 12, pp. 4082–4090, 1998.

[5] Y. Hu, S. Yurkovich, Y. Guezennec, and B. Yurkovich, "Electro-thermal battery model identification for automotive applications," *Journal of Power Sources*, vol. 196, pp. 449–457, 2011.

[6] P. Liu, J. Wang, J. Hicks-Garner, E. Sherman, S. Soukiazian, M. Verbrugge, H. Tataria, J. Musser, and P. Finamore, "Cycle-life model for graphite-LiFePO$_4$ cells," *Journal of Power Sources*, vol. 196, pp. 3942 – 3948, 2011.

[7] V. Marano, S. Onori, Y. Guezennec, G. Rizzoni, and N. Madella, "Lithium-ion batteries life estimation for plug-in hybrid electric vehicles," ser. Proceedings of the Vehicle Power and Propulsion Conference, Dearborn, MI, U.S.A., 2009.

[8] J. Marcicki, G. Rizzoni, A. Conlisk, and M. Canova, "A reduced-order electrochemical model of lithium-ion cells for system identification of battery aging," ser. Proceedings of the 4th Annual Dynamic Systems and Control Conference, Arlington, VA, U.S.A., Oct 2011.

[9] J. Newman and K. Thomas-Alyea, *Electrochemical Systems, 3rd Edition*. Hoboken, NJ: John Wiley and Sons, Inc., 2004.

[10] P. Ramadass, B. Haran, P. Gomadam, R. White, and B. Popov, "Development of first principles capacity fade model for li-ion cells," *Journal of the Electrochemical Society*, vol. 151, no. 2, pp. A196 – A203, 2004.

[11] M. Roscher and D. Sauer, "Dynamic electric behavior and open-circuit-voltage modeling of LiFePO$_4$-based lithium ion secondary batteries," *Journal of Power Sources*, vol. 196, pp. 331 – 336, 2011.

[12] M. Safari and C. Delacourt, "Modeling of a Commercial Graphite/LiFePO$_4$ Cell," *Journal of The Electrochemical Society*, vol. 158, no. 5, pp. A562 – A571, 2011.

[13] S. Santhanagopalan, Q. Guo, P. Ramadass, and R. White, "Review of models for predicting the cycling performance of lithium ion batteries," *Journal of Power Sources*, vol. 156, pp. 620–628, 2006.

[14] S. Santhanagopalan, Q. Zhang, K. Kumaresan, and R. White, "Parameter Estimation and Life Modeling of Lithium-Ion Cells," *Journal of the Electrochemical Society*, vol. 155, no. 4, pp. A345 – A353, 2008.

[15] A. Schmidt, M. Bitzer, A. Imre, and L. Guzzella, "Experiment-driven electrochemical modeling and systematic parameterization for a lithium-ion battery cell," *Journal of Power Sources*, vol. 195, pp. 5071–5080, 2010.

[16] Z. Shi, Z. Xu, and J. Co, "The convergence of subspace trust region methods," *Journal of Computational and Applied Mathematics*, vol. 231, no. 1, pp. 365 – 377, 2009.

[17] C. Speltino, D. Domenico, G. Fiengo, and A. Stefanopoulou, "Comparison of Reduced Order Lithium-Ion Battery Models for Control Applications," ser. Proceedings of the 48th IEEE Conference on Decision and Control, 2009 held jointly with the 2009 28th Chinese Control Conference, Shanghai, P.R. China, Dec 2009, 3276-3281.

[18] K. Thomas-Alyea, "Modeling Resistive Reactant and Phase-Change Materials in Battery Electrodes," *ECS Transactions*, vol. 16, no. 13, pp. 155 – 165, 2008.

[19] J. Wang, J. Hicks-Garner, E. Sherman, S. Soukiazian, M. Verbrugge, H. Tataria, J. Musser, P. Finamore, and P. Liu, "Aging Mechanisms of LiFePO$_4$ Batteries Deduced by Electrochemical and Structural Analyses," *Journal of the Electrochemical Society*, vol. 157, no. 4, pp. A499 – A507, 2008.

TABLE V: Nomenclature used in this work.

Parameter	Definition
A	current collector area (m^2)
a	specific surface area of electrode (m^2/m^3)
c	lithium concentration (mol/m^3)
c_{max}	saturation concentration of Li$^+$ in active material[c]
D	effective diffusion coefficient (m^2/s)
e	error between model and experimental measurement (V)
F	Faraday constant (C/mol)
H	maximum hysteresis magnitude (V)
I	external current (A)
j	intercalation current density (A/m^3)
k	intercalation reaction rate constant (A m^5/mol$^{3/2}$)
L	thickness of a domain (m)
L_p	empirical resistive reactant parameter
P	generic model parameter for the sensitivity study
Q	cell capacity (Ah)
R_c	contact resistance (Ω)
R_r	resistive reactant resistance (Ω)
$\bar{R}$	universal gas constant (J/mol K)
T	temperature (K)
t_0^+	transference number of Li$^+$
U	open-circuit voltage of electrode relative to Li/Li$^+$ (V)
V	terminal voltage (V)
V_h	hysteresis overpotential (V)
x	spatial coordinate (m)
y_0	initial degree of cathode intercalation[c]
z_0	initial degree of anode intercalation[c]
α	Butler-Volmer transfer coefficient (assumed 0.5)
β	activity coefficient of Li$^+$ in liquid
ϵ	active material volume fraction
η	charge transfer overpotential (V)
σ	conductivity (S/m)
τ_H	hysteresis time constant (s)
ϕ	potential (V)
e	subscript denoting liquid phase
i	subscript denoting electrode property ($i = an$ or $i = ca$)
n	subscript denoting negative electrode
p	subscript denoting positive electrode
s	subscript denoting solid phase